Pis'ma v ZhETF, vol. 104, iss. 5, pp. 334 – 335

Transport of Electrons on Liquid Helium in a Microchannel Device near the Current Threshold

N. R. Beysengulov[+*1)], *D. G. Rees*[*×], *D. A. Tayurskii*[+*], *K. Kono*[+*×]

[+]*KFU-RIKEN Joint Research Laboratory, Institute of Physics, Kazan Federal University, 420008 Kazan, Russia*

[*]*RIKEN CEMS, 351-0198 Wako, Japan*

[×]*NCTU-RIKEN Joint Research Laboratory, Institute of Physics, National Chiao Tung University, 300 Hsinchu, Taiwan*

Submitted 25 July 2016

DOI: 10.7868/S0370274X16170082

Surface-state electrons (SSE) trapped on the surface of liquid helium represent the simplest example of a strongly interacting Coulomb system [1, 2]. A unique interaction between electron and helium medium results in a quantisation of the electron motion perpendicular to the surface. At low temperatures, electrons occupy only the ground level, forming a pure two-dimensional (2D) system. SSE on liquid helium provide a unique system for studying classical and quantum-mechanical phenomena in mesoscopic dimensions. The SSE density range $10^8-10^9\,\mathrm{cm}^2$ gives a typical interelectron separation of $0.5-1\,\mu$m. Such length scales are accessible using modern nanofabrication techniques. This has led to an increased activity in investigations of the properties of small ensembles of SSE in microstructured devices, the sizes of which can be made comparable with interelectron distance. Generally, geometrical confinement results in an enhancement of correlated electron behaviour in low-dimensional systems [3]. For example, the transport of single electrons through a split-gate constriction revealed conductance steps related to electron row formation [4, 5], a classical analog of the quantum point contacts. The formation of electron, or Wigner, crystals just a few electron rows wide in microchannel geometries has been studied using transport measurements [6, 7]. Strong electrostatic confinement, comparable in strength with Coulomb interactions in the SSE system, is essential to observe these effects. However, the influence of electrostatic confinement on the electron transport close to the threshold point remains only partially understood. Here we present transport measurements of q1D SSE in microchannel devices close to the conductance threshold point.

In this work we study two devices S1 and S2 prepared using standard UV-lithography techniques [8, 9]. Figure 1a shows an image of the central area of the device. The device consists of 2 sets of microchannel arrays, which are used as SSE reservoirs. The microchannels are formed by a 100 nm-thick bottom Reservoir Electrode and top Guard electrodes made from Au, separated by insulating hard-baked photoresist. The two reservoirs are connected by a smaller 100 μm-long central microchannel (CM). The CM is formed by Split Gate (SG) and Bottom Gate (BG) electrodes, with

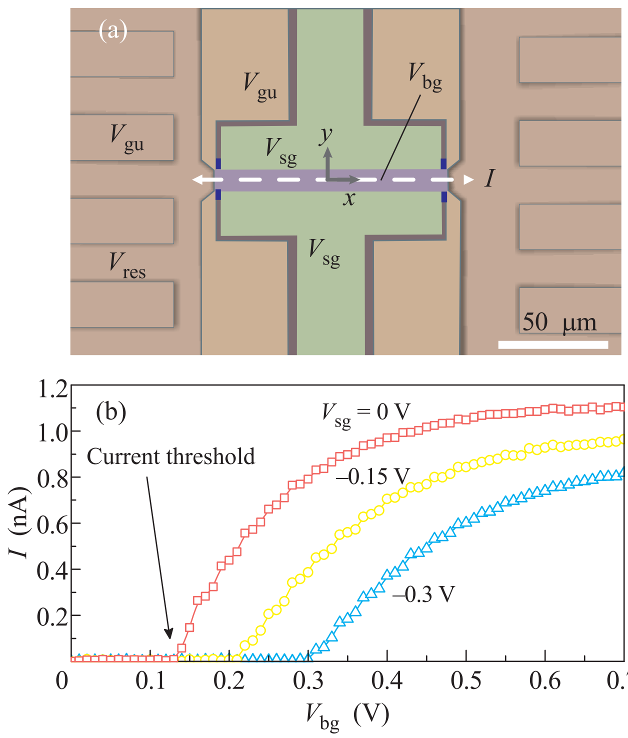

Fig. 1. (Colour online) (a) – Optical microscope image of the device S1 used for SSE transport measurements. Similar device was used in [8]. The dashed horizontal arrow indicates the direction of the electron motion (and measured electric current). (b) – Characteristic electric current I versus V_{bg} dependence at 3 different V_{sg} values for the sample S1. Here $T = 1.3\,\mathrm{K}$, $V_{ac} = 2.1\,\mathrm{mV}$

[1)]e-mail: n.beysengulov@gmail.com

channel width $W = 7(10)\,\mu$m and depth $d = 1.9(1.6)\,\mu$m for the device S1 (S2). The lateral electrostatic confinement in the CM is formed by applying $V_{\rm bg}$ and $V_{\rm sg}$ voltages on BG and SG electrodes, respectively. Voltages $V_{\rm res}$ and $V_{\rm gu}$ are applied to the Reservoir and Guard electrodes, respectively, to hold electrons in the reservoirs. Experiments were performed at temperature $T = 1.3$ K. The microchannels are filled with superfluid ^{4}He by capillary action. SSE are generated by thermionic emission from a tungsten filament placed above the device. A modulation of the voltage on the Left Reservoir electrode with an ac-signal of small amplitude $V_{\rm ac}$ and frequency $f = 201$ kHz induces a charge flow between the reservoirs. The electric current induced in the Right Reservoir electrode I is detected using standard ac lock-in techniques. The circuit is well described by a lumped-circuit RC model [10]. To understand our data quantitatively, we use FEM technique to calculate the average areal density n_s, the linear density n_l, the effective width of the electron system in the channel w_e and the shape of the electrostatic confinement $\phi(y)$ [11, 12].

According to electrostatic model, electrons are unable to move through the CM when the electrostatic potential at the channel centre ϕ_0 becomes more negative than the electrostatic potential of electrons in the reservoirs ϕ_e. ϕ_0 is controlled by $V_{\rm bg}$ and $V_{\rm sg}$, and, by increasing $V_{\rm bg}$, becomes more positive. Above the threshold value electrons enter the CM and, on increasing $V_{\rm bg}$ further, the number of charge carriers increases in the CM. This leads to the increase in the measured electric current, as it shown in Fig. 1b. Examination of the electrostatic potential map across the device using FEM analysis reveals that the minimum of $\phi(x, y = 0)$ usually appears at the centre of CM. In this case the threshold points are defined for the point $x = 0$. However, under some conditions, the minimum of $\phi(x, y = 0)$ shifts to the edges of the CM, where the influence from the other electrodes modifies the threshold conditions. We show that FEM predictions of threshold conditions are consistent with experimental data for both devices and underline the significance of the device geometry.

Experiments show that electric current $I(V_{\rm sg})$ varies smoothly above the current threshold $V_{\rm sg} > V_{\rm sg}^{\rm th}$, as predicted by the charge continuum model. However, an abrupt drop of the current signal occurs at the threshold point that is not consistent with this model. Here, at the current threshold, the charge continuum model is expected to break down due to extremely low electron densities. The observed signal jump can be considered a consequence of the granular nature of charges. In this case, transport through the CM is allowed when the charging energy of the CM area is overcome. We found charging energy $E_C = e \times 17$ mV under a simple capacitor approximation, which defines the energy required to charge a square area $w_e \times w_e$ with one electron. As a consequence, a single chain of electrons is formed at the current threshold point with a finite linear density $n_l = 1/w_e$. Finally, we investigate the charging voltage $\Delta V_{\rm sg}$ at different confinement parameters. We find a good agreement between experimental data and the results of FEM calculations of $N_y = 1$ condition, which supports our interpretation of the data in terms of charging energy effects.

The observation of this classical charging effect for a single electron chain is quite unique. We are not aware of any other examples of this effect. We are able to observe it here due to the nondegenerate and strongly interacting nature of the electron system. In addition, the helium substrate is perfectly clean and so transport measurements can be performed at extremely low electron densities. This is in contrast with low dimensional systems in solid state devices for which pinning by impurities typically restricts transport measurements when the electron density is low.

Full text of the paper is published in JETP Letters journal.

DOI: 10.1134/S002136401617001X

1. E. Y. Andrei, *Two-Dimensional Electron Systems on Helium and Other Cryogenic Substrates*, Kluwer Academic Publishers, Dordrecht (1997).
2. Yu. P. Monarkha and K. Kono, *Two-Dimensional Coulomb Liquids and Solids*, Springer-Verlag, Berlin (2004).
3. V. V. Deshpande, M. Bockrath, L. I. Glazman, and A. Yacoby, Nature **464**, 7286, 209 (2010).
4. D. G. Rees, I. Kuroda, C. A. Marrache-Kikuchi, M. Höfer, P. Leiderer, and K. Kono, Phys. Rev. Lett. **106**, 2, 026803 (2011).
5. D. G. Rees, H. Totsuji, and K. Kono, Phys. Rev. Lett. **108**, 17, 176801 (2012).
6. H. Ikegami, H. Akimoto, D. G. Rees, and K. Kono, Phys. Rev. Lett. **109**, 23, 236802 (2012).
7. D. G. Rees, H. Ikegami, and K. Kono, J. Phys. Soc Jpn. **82**, 124602 (2013).
8. D. G. Rees, N. R. Beysengulov, J.-J. Lin, and K. Kono, Phys. Rev. Lett **116**, 20, 206801 (2016).
9. D. G. Rees, I. Kuroda, C. A. Marrache-Kikuchi, M. Höfer, P. Leiderer, and K. Kono, J. Low Temp. Phys. **166**, 3, 107 (2012).
10. Y. Iye, J. Low Temp. Phys. **40**, 441 (1980).
11. N. R. Beysengulov, D. G. Rees, Y. Lysogorskiy, N. K. Galiullin, A. S. Vazjukov, D. A. Tayurskii, and K. Kono, J. Low Temp. Phys. **182**, 28 (2016).
12. F. Hecht, J. Numer. Math. **20**, 251 (2012).